Astronomy & Astrophysics manuscript no. laboca˙rev2
October 19, 2010

X-ray observations of sub-mm LABOCA galaxies in the eCDFS

I. Georgantopoulos[1,2] E. Rovilos[3] A. Comastri[1]

[1] INAF-Osservatorio Astronomico di Bologna, Via Ranzani 1, 40127, Italy

[2] Institute of Astronomy & Astrophysics, National Observatory of Athens, Palaia Penteli, 15236, Athens, Greece

[3] Max Planck Institut für extraterrestrische Physik, Giessenbachstraße, 85748 Garching, Germany

Received ; accepted

ABSTRACT

We explore the X-ray properties of the 126 sub-mm galaxies (SMGs) of the LABOCA survey in the CDFS and the eCDFS regions. SMGs are believed to experience massive episodes of star-formation. Our goal is to examine whether star-formation coexists with AGN activity, determine the fraction of highly obscured AGN and finally to obtain an idea of the dominant power-mechanism in these sources. Using Spitzer and radio arc-second positions for the SMGs, we find 14 sources with significant X-ray detections. For most of these there are only photometric redshifts available, with their median redshift being ~ 2.3. Taking into account only the CDFS area which has the deepest X-ray observations, we estimate an X-ray AGN fraction of $< 26 \pm 9$ % among SMGs. The X-ray spectral properties of the majority of the X-ray AGN which are associated with SMGs are consistent with high obscuration, $> 10^{23}\,\mathrm{cm}^{-2}$, but there is no unambiguous evidence for the presence of Compton-thick sources. Detailed Spectral Energy Distribution fittings show that the bulk of total IR luminosity originates in star-forming processes, although a torus component is usually present. Finally, stacking analysis of the X-ray undetected SMGs reveals a signal in the soft (0.5-2 keV) and marginally in the hard (2-5 keV) X-ray band. The hardness ratio of the stacked signal is relatively soft (-0.40 ± 0.10) corresponding to $\Gamma \sim 1.6$. This argues against a high fraction of Compton-thick sources among the X-ray undetected SMGs.

Key words. X-rays: general; X-rays: diffuse background; X-rays: galaxies; submillimeter: galaxies

1. Introduction

The advent of the SCUBA detector (Holland et al. 1999) on the James Clerk Maxwell Telescope has brought a spectacular advance in the field of sub-mm cosmology. The first extragalactic surveys at 850 μm revealed a population of numerous luminous high redshift sub-millimeter galaxies or SMGs (see Blain et al. 2002 for a review). Sub-mm surveys are very fruitful in detecting distant galaxies because of the negative K-correction at sub-mm wavelengths which counteracts the dimming of light with increasing distance. The SMGs generate significant fractions of the energy produced by all galaxies over the history of the Universe (e.g. Smail, Ivison & Blain 1997, Barger et al. 1998, Hughes et al. 1998, Blain et al. 1999, Arexatga et al. 2007, Wall, Pope & Scott 2008), being probably among the most luminous objects in the Universe. The limited spatial resolution at sub-mm wavelengths has hampered the identification of their optical counterparts. Recently, Chapman et al. (2003, 2005) have made great advances by identifying a large number of SMGs through their radio counterparts and subsequently following them with Keck spectroscopy. These studies have shown that the SMG population lies at high redshift with the median being z=2-3, (see also Maiolino 2008 and references therein), although the highest redshift SMGs have been found out to z$\sim 4-5$ (Capak al. 2008, Daddi et al. 2009, Coppin et al. 2009, Wardlow et al. 2010).

Mid-IR spectroscopy with Spitzer IRS reveals mainly star-forming spectra with implied star-formation rates as high as $1000\,\mathrm{M}_{\odot}\,\mathrm{yr}^{-1}$ (Valiante et al. 2007, Pope et al. 2008, Menendez-Delmestre et al. 2007, 2009). Pope et al. (2008) obtained IRS spectra of 13 SMGs in the CDFN: 11 of these were detected with their spectra being dominated by PAH features. Given the known anti-correlation between PAH emission and AGN activity this directly suggests that star-formation is the major powering mechanism in these SMGs. The median luminosity of these powerful star-forming galaxies approaches $1 \times 10^{13}\,\mathrm{L}_{\odot}$ at a median redshift of z=2.7.

The X-ray data have identified many AGN among SMGs. Alexander et al. (2005a, 2005b) have found X-ray counterparts to a sample of 20 SMGs with radio counterparts from Chapman et al. (2005) in the Chandra Deep Field North (CDFN). Based on the number of X-ray detections, Alexander et al. (2005b) claim a high fraction ($75 \pm 19\%$) of AGN among the sub-mm galaxies which have radio counterparts. If one takes into account the radio undetected SMGs in the CDFN, making the conservative assumption that none of the radio undetected SMGs hosts AGN activity, then the AGN fraction in the SMG population becomes $> 38^{+12}_{-10}$ % (Alexander et al. 2005a). Alexander et al. (2005b) claim that the vast majority of the radio-detected SMGs are highly obscured with column densities exceeding $10^{23}\,\mathrm{cm}^{-2}$. The above results suggest that

Send offprint requests to: I. Georgantopoulos, e-mail: ioannis.georgantopoulos@oabo.inaf.it

in SMGs the intense star-formation goes hand in hand with the supermassive black-hole growth. The low L_X/L_{FIR} ratio suggests that intense star-formation activity dominates the bolometric output (Alexander et al. 2005b). Laird et al. (2010) presented an analysis of 35 SMGs in the CDFN with sub-arcsec positions either from radio or *Spitzer* counterparts. They find 16 objects with significant X-ray detection, or a fraction of about 45 ± 8 %. However, they find that a dominant AGN contribution is only required in only seven sources, or 20% of the SMG sample. This figure lies at the lower limit of previous estimates raising questions on how common the AGN contribution in sub-mm galaxies is.

Recently, the LABOCA sub-mm camera on the APEX telescope has performed a sensitive sub-mm survey of the CDFS and its environs, that is the extended CDFS (eCDFS). The CDFS is the region of the sky with the deepest X-ray data available (together with the CDFN) and thus provides the opportunity to further explore the X-ray properties of SMGs. Lutz et al. (2010) have performed a stacking analysis in the sub-mm LABOCA map of the X-ray sources detected in the eCDFS. Their main aim is to explore the star-formation properties of the X-ray AGN population as revealed by its sub-mm emission. In this paper, in a complementary study we explore the X-ray properties of the SMGs in the LABOCA survey. Our goal, in analogy with the work of Alexander et al. (2005a) and Laird et al. (2010) in the CDFN, is to study the fraction of AGN among SMGs and in particular the fraction of heavily obscured sources and Compton-thick AGN among them. Hereafter, we adopt $H_o = 75\,km\,s^{-1}\,Mpc^{-1}$, $\Omega_M = 0.3$, $\Omega_\Lambda = 0.7$ throughout the paper.

2. Data

2.1. The LABOCA sub-mm survey

LABOCA is the sub-millimeter camera (Siringo et al. 2009) at the APEX telescope (Güsten et al. 2006). We use the 870 μm map obtained by the LABOCA eCDFS sub-mm survey -LESS- (Weißet al. 2009). LESS covers the full 30×30 arcmin field size of the eCDFS and has a uniform noise level of $\sigma_{870\mu m} \approx 1.2$mJy/beam. This catalog contains 126 sources detected at $> 3.7\sigma$. Simulations show that at the above extraction limit, 95% of the sources have positional accuracy better than 8 arcsec (Weißet al. 2009).

2.2. X-ray Data

The 2Ms CDFS observations consist of 23 pointings. The analysis of the 1 Ms data is presented in Giacconi et al. (2002) and Alexander et al. (2003) while the analysis of all 23 observations is presented in Luo et al. (2008). The average aim point is $\alpha = 03^h32^m28^s.8$, $\delta = -27°48'23''$ (J2000). The 23 observations cover an area of 435.6 arcmin^2. 462 X-ray sources have been detected by Luo et al. (2008). The CDFS survey reaches a sensitivity limit of 1.3×10^{-16} erg cm^{-2} s^{-1} and 1.9×10^{-17} erg cm^{-2} s^{-1} in the hard (2-8 keV) and soft (0.5-2 keV) band respectively. This corresponds to a false-positive probability threshold of 10^{-6} (see Luo et al. 2008). The Galactic column density towards the CDFS is 0.9×10^{20} cm^{-2} (Dickey & Lockman 1990).

The eCDFS consists of four contiguous 250 ks *Chandra* observations covering ≈ 0.3 deg^2 centered on the CDFS. Source detection has been performed by Lehmer et al. (2005) and Virani et al. (2006). Here, we use the source detection of Lehmer et al. (2005) in which 762 sources have been detected. The sensitivity limit reaches 1.1×10^{-16} and 6.6×10^{-16} erg cm^{-2} s^{-1} in the 0.5-2 and 2-8 keV bands respectively. This corresponds to a false-positive probability threshold of 10^{-6}.

2.3. Mid-IR

The central regions of the CDFS have been observed in the mid-IR by the *Spitzer* mission (Werner 2000) as part of the Great Observatory Origin Deep Survey (GOODS). These observations cover areas of about 10×16.5 arcmin^2 in both fields using the IRAC (3.6, 4.5, 5.8 and 8.0 μm) and the MIPS (24 μm) instruments onboard *Spitzer*. The sensitivity is 80 μJy (5σ) in the 24 μm MIPS band. The data products are available from the *Spitzer* data centre (http://data.spitzer.caltech.edu/popular/goods/).

For the extended region bracketing the GOODS area we have used data from *Spitzer*'s IRAC and MUSYC Public Legacy of the eCDFS (SIMPLE[1], see van Dokkum et al. 2005) and the Far-Infrared Deep Extragalactic Legacy survey (FIDEL[2], see Magnelli et al. 2009). SIMPLE is an IRAC survey of a 0.5×0.5 deg area centered on the CDFS. The source catalogue contains more than 60000 sources with an exposure time ranging from 2 to 4 hours and a flux limit of ~ 24 mag(AB) in the 3.6 μm band. FIDEL is a MIPS survey of the eCDFS with a median exposure time of 8000 s in the 24 μm band and in the 30×30 arcmin area of the eCDFS. We note that the area of the eCDFS has been also observed with the *Herschel* far-IR mission (e.g. Shao et al. 2010) but the data are not yet publicly available.

2.4. Optical Data

The CDFS has been imaged extensively in the optical (e.g. Giacconi et al. 2002). In this paper we are making use of the CTIO-4 m-MOSAIC II camera observations (Gawiser et al. 2006) taken as part of the MUSYC project. The survey is complete to a total magnitude of R=25(AB).

3. Sample Selection

A simple cross-correlation between the positions of the 126 LABOCA sources with those of X-ray sources from the catalogues of Luo et al. (2008) and Lehmer et al. (2005) in the CDFS and eCDFS fields respectively, reveals 20 possible associations, using a search radius of 8″, the same as the minimum positional accuracy of the LABOCA catalogue. In order to select the most reliable LABOCA - X-ray counterparts and identify any possible chance encounters, we use the mid-infrared emission from IRAC and MIPS, whose images have a much higher source density than those of LABOCA and *Chandra* .

We first cross-match the positions of the LABOCA sources with the positions of the 24 μm *Spitzer* MIPS sources. We choose this band as it is expected that there will be a correlation between the sub-mm emission and that at mid-IR wavelengths (Pope et al. 2006). We use the likelihood ratio (LR) method (Sutherland & Saunders 1992)

[1] http://www.astro.yale.edu/dokkum/SIMPLE/
[2] http://www.noao.edu/noao/fidel/

to select the most probable counterpart, choosing the optimum likelihood ratio threshold that maximizes the sum of reliability and recovery fraction (see Luo et al. 2010, Rovilos et al. 2010). Starting with an initial search radius of $8''$and with $LR > 0.4$ we find MIPS counterparts for 87% of the LABOCA sources which fall in the area mapped by FIDEL, with a mean reliability of 70%. Among the LABOCA - MIPS associations are 18/20 LABOCA sources with an X-ray counterpart. We then check the positions of the X-ray sources on the FIDEL map to look for any X-ray sources which are associated with a $24\,\mu$m source which is not the most probable counterpart to the LABOCA source; we find one such case, which we remove from our sample. We repeat the above procedure using the IRAC catalogue and map (from the SIMPLE survey) to investigate the two LABOCA - X-ray sources with no MIPS association. We find that the IRAC source associated with the X-rays is not the most probable counterpart to the LACOCA source in both cases, and remove them from our sample. We also check the positions of the radio (VLA - 20cm) sources of Kellerman et al. (2008) at a flux limit of 43 mJy (5σ). We find radio counterparts for 5/18 LABOCA - X-ray associations (40, 57, 67, 108, 114); their radio positions agree with the FIDEL positions within $1.4''$.

The final step is to check the optical images. In Fig. 1 we plot the MUSYC images of the 17 LABOCA - X-ray candidates. With circles (3 arcsec radius) we mark the MIPS positions, while the X-ray sources are marked with crosses, prefering the CDFS 2 Ms positions to the eCDFS, in cases when a source is detected in both surveys. The images are centred in the LABOCA positions with a 25 arcsec size. The number on the top-left of each image is the LABOCA identification. We can clearly see that there are two cases where the X-ray source is more likely to be associated with a different optical source than the one producing the bulk of the $24\,\mu$m flux: these are W-107 and W-111. In the case of W-107, the $24\,\mu$m flux is coming from three discrete optical sources and the X-ray source is associated with the one which lies farther away from the LABOCA position. Therefore it is highly unlikely that the X-rays and the sub-mm emissions are physically connected. In the case of W-111 the X-ray source is different than the $24\,\mu$m source and again the X-ray and the sub-mm emissions are not associated. We remove both sources from our sample.

We note that the X-ray counterpart of one source (W-96) is flagged as a star in Taylor et al. (2009). We check its optical morphology using *HST* imaging from the GEMS survey (Rix et al. 2004) and we confirm that it has an unresolved morphology with a PSF of $\sim 0.08''$ (diffraction limit in the z_{850} band). The X-ray to optical flux ratio is low ($\log[f_{0.5-2\,\mathrm{keV}}/f_R] = -1.8$) confirming the stellar classification (see e.g. Rovilos et al. 2009). On these grounds we remove this source from the final sample. This of course does not suggest that this is a star having sub-mm emission, but simply that the X-rays are related to a stellar source, while there is no association of the sub-mm source with an X-ray extragalactic source.

Our final sample consists of 14 sources. Ten of them are in the region observed by the 2 Ms CDFS and four are in the shallower eCDFS region. The mean reliability of the sub-mm - MIPS associations for these 14 sources is 87.5%, i.e. we expect 1.7 spurious sources in our sample.

4. Photometry and redshifts

For the photometry in the optical bands we use the MYSYC catalogues of Taylor et al. (2009) and Gawiser et al. (2006). Taylor et al. (2009) provide photometry of ~ 17000 sources of the eCDFS detected in the (CTIO-4 m - ISPI) K-band in the $U-B-V-R-I-z'-J-H-K$ bands, and Gawiser et al. (2006) use the same optical data to detect sources in the combined $B-V-R$ band and provide photometry in the $U-B-V-R-I-z'$ bands.

The *Spitzer* photometry comes from the SIMPLE and FIDEL surveys. In the public SIMPLE catalogue the aperture fluxes are given, and we use the $2''$ apertures and standard aperture corrections derived from the IRAC cookbook[3] to calculate the total fluxes. In the FIDEL case we use the corrected isophotal fluxes derived from the *SEXTRACTOR* source detection code (Bertin & Arnouts 1996). We identify as a source an accumulation of 6 pixels with flux higher than 1.5 times the local rms. We calibrate the derived fluxes using the total fluxes of common sources between the FIDEL and MIPS-GOODS surveys. We also visually inspect the apertures derived from *SEXTRACTOR* to check for source blending problems, and also to check if they include all the flux of the source, since the MIPS PSF has prominent side-lobe features. We find only one such case (W-108), where the aperture used does not encompass all the flux and we consider the measured flux as a lower limit.

Three sources in our sample (W-40, W-45, and W-67) fall in the area of GOODS which has a deeper coverage with IRAC and MIPS, as well as the *HST*. For these sources we use the photometry of Grazian et al. (2006) which includes optical and IRAC bands. These three, along with sources 9 and 11 fall in the MIPS-GOODS area with deeper coverage than FIDEL, and therefore we use the GOODS $24\,\mu$m photometry.

As a final step, we inspect the images of the 14 LABOCA - X-ray sources in all the bands used and compare them with with those with the smallest PSF; the optical GEMS images and (where available) the GOODS-*HST* images. We do that in order to detect whether the flux measured in the bands with the larger PSFs are blended with nearby sources. We find that sources W-59 and W-67 are in fact double sources blended in the IRAC and MIPS images because of limited spatial resolution, whereas for sources 9, 40, and 84 there are nearby sources which affect the MIPS flux. Source 67 is in the GOODS area and has optical and IRAC photometry from the GOODS-MUSYC survey Grazian et al. (2006), which uses PSF matching to the *HST* images to measure the fluxes in the optical and infrared bands, so we consider the problem to be confined only in the MIPS photometry (taken from GOODS).

Four sources (W-57, W-67, W-108, and W-114) have spectroscopic redshifts assigned to their optical, infrared, or radio counterparts: Szokoly et al. (2004), Kriek et al. (2006), Norris et al. (2006), Chapin et al. (2010) respectively. The photometric redshifts in the area of the CDFS come from Luo et al. (2010), where photometric redshifts are calculated for X-ray sources using up to 42 UV, optical, and infrared bands. The photometric redshifts in the area of the eCDFS come from Taylor et al. (2009). Finally, the photometric redshift of source W-4 in the eCDFS is calcu-

[3] http://ssc.spitzer.caltech.edu/irac/iracinstrumenthandbook/

lated using the EAZY (Brammer et al. 2008) code using the B, V, R, I, and z' bands. This source does not have a photometric redshift in the K-selected sample of Taylor et al. (2009) as it has not been detected in this band. In Table 1 we present the X-ray, optical, and infrared fluxes as well as the available redshifts of the sources in our sample.

5. X-ray Properties

The X-ray properties can give a first idea on the nature of the X-ray detected SMGs. X-ray luminosities higher than about a few times $10^{42}\,\mathrm{erg\,s^{-1}}$ are usually attributed to AGN activity. This limit has been dictated by the highest X-ray luminosity observed in local star-forming galaxies (e.g. Zezas, Georgantopoulos & Ward 1998, Moran, Lehnert & Helfand 1999). However, given that SMGs are probably the most powerful star-forming systems it is not unlikely that their X-ray luminosity may surpass this limit. Star-forming systems present very little, if any obscuration (e.g. Georgakakis et al. 2006, 2007, Tzanavaris et al. 2006, Rovilos et al. 2009 and references therein). Therefore the detection of a substantial obscuring column, through X-ray spectroscopy in a low X-ray luminosity source can further differentiate between a star-forming galaxy and an AGN.

5.1. X-ray spectroscopy

We use the *SPECEXTRACT* script in the CIAO v4.2 software package to extract the spectra of the 14 X-ray sources in our sample. The extraction radius varies between 2 and 4 arcsec with increasing off-axis angle. At low off-axis angles (<4 arcmin) this encircles 90% of the light at an energy of 1.5 keV. The same script extracts response and auxiliary files. The addition of the spectral, response and auxiliary files has been performed with the FTOOL tasks *MATHPHA*, *ADDRMF* and *ADDARF* respectively. We use the C-statistic technique (Cash 1979) specifically developed to extract spectral information from data with low signal-to-noise ratio. We use the XSPEC v12.5 software package for the spectral fits (Arnaud 1996).

We fit the data using a power-law absorbed by a cold absorber. We treat both the intrinsic column density and the photon index (Γ) as free parameters. However, in five cases the photon statistics are low, not allowing us to derive meaningful constraints for both $N_{\rm H}$ and Γ. In these cases we can only fix the power-law photon index to $\Gamma = 1.8$ (Nandra & Pounds 1994, Tozzi et al. 2006), leaving only the column density $N_{\rm H}^{\rm eff}$ as the free parameter and vice-versa i.e. setting $N_{\rm H} = 0$ and leaving the photon index $\Gamma^{\rm eff}$ as a free parameter. The spectral-fit results are presented in Table 2. As it is customary in X-ray Astronomy, errors correspond to the 90% confidence level.

5.2. AGN vs. star-forming galaxies

In Fig. 2 we plot the effective photon index as a function of the obscured X-ray luminosity, i.e. column (7) vs. column (8) in Table 2. We see that nine sources have high X-ray luminosities ($> 10^{43}$ erg s^{-1}) and thus can be considered as bona-fide AGN. Four out of the remaining low luminosity sources present soft spectra and thus are possibly associated with star-forming galaxies. The remaining source (W-114) has a hardish spectrum and thus could be a highly obscured AGN: its spectrum is marginally intrinsically flat ($\Gamma < 1.32$ at the 90% confidence level) and thus possibly associated with a Compton-thick AGN with a reflection dominated spectrum.

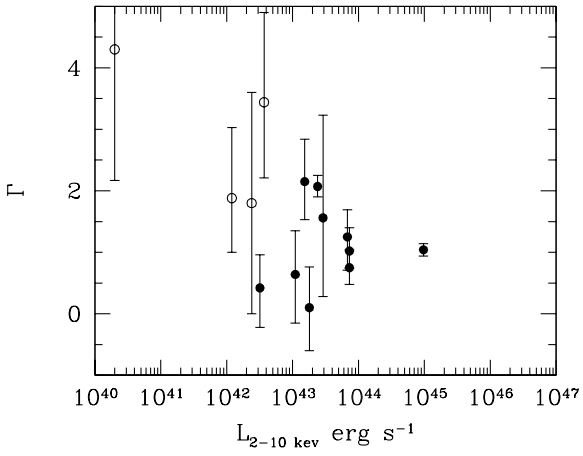

Fig. 2. The effective photon index as a function of X-ray luminosity. Filled and open circles correspond to AGN and galaxies respectively (see text).

5.3. X-ray obscuration

In Fig. 3 we plot the distribution of the rest-frame column densities (column 6 in table 2). It is evident that most AGN (7/10) present column densities exceeding $10^{23}\,\mathrm{cm^{-2}}$, i.e. they are characterised as heavily obscured AGN. One source could be a transmission dominated Compton-thick AGN (W-11). However, the uncertainty in the photometric redshift certainly makes this classification dubious.

6. Mid-IR properties

6.1. Mid-IR Spectral Energy Distributions

We construct the spectral energy distribution (SED) in order to obtain an idea on the dominant powering mechanism (AGN or star-formation) in the mid-IR part of the spectrum. The SEDs are also used in order to obtain an accurate estimate of the infrared luminosities. Power-law SEDs in the mid-IR are characteristic of AGN emission (e.g. Alonso-Herrero et al. 2006, Polletta et al. 2007). A prototype power-law mid-IR SED in the local Universe is that of Mkn231 (Armus et al. 2007). This is a broad-absorption-line QSO (Braito et al. 2004) and a Ultraluminous Infrared IRAS galaxy. On the other hand star-forming sources have a distinct dip in their mid-IR spectra at a rest-frame wavelength below 10 μm. Such a source is Arp 220 (e.g. Iwasawa et al. 2005), a ULIRG whose far-IR SED is dominated by a very strong star-forming component (Armus et al. 2007). We present the IRAC/MIPS SEDs in Fig. 4. There are only two clearcut power-law SEDs suggestive of AGN: W-4 and W-57.

Table 1. Photometry

ID	α	δ	$f_{0.5-10\,keV}$	R	$f_{3.6\,\mu m}$	$f_{24\,\mu m}$	$f_{850\,\mu m}$	LR	z	Ref.
(1)	(2)	(2)	(3)	(4)	(5)	(6)	(7)	(8)	(9)	(10)
W-4	52.8996	-27.9121	1.85	24.94	7.00 ± 0.10	139 ± 5	11.0 ± 1.2	5.00	2.58 ± 0.9	1
W-9	53.0475	-27.8704	7.14	26.02	9.83 ± 0.05	122 ± 5 [b]	9.4 ± 1.2	6.92	3.99 ± 0.08	2
W-11	53.0577	-27.9334	1.33	25.61	6.83 ± 0.07	113 ± 6	9.2 ± 1.2	5.06	6.07 ± 1.1	2
W-40	53.1950	-27.8557	0.44	24.35	8.51 ± 0.15	140 ± 4 [b]	6.4 ± 1.2	6.08	1.90 ± 0.02	2
W-45	53.1052	-27.8752	0.06	27.41	7.50 ± 0.27	141 ± 4	6.3 ± 1.2	1.50	2.50 ± 0.2	2
W-57	52.9665	-27.8908	1.51	24.33	7.60 ± 0.10	273 ± 6	6.1 ± 1.3	12.81	2.940	3
W-59	53.2658	-27.7362	1.35	25.62	30.28 ± 0.10 [a]	453 ± 5 [a]	6.0 ± 1.3	7.67	1.38 ± 0.02	2
W-66	53.3830	-27.9028	36.1	20.72	56.34 ± 0.13	679 ± 9.4	6.1 ± 1.3	5.37	0.58 ± 0.03	5
W-67	53.1803	-27.9206	0.29	24.20	21.7 ± 0.9	554 ± 4 [a]	5.9 ± 1.3	15.77	2.122	4
W-84	52.9773	-27.8513	1.58	24.97	12.98 ± 0.09	231 ± 4 [b]	5.5 ± 1.3	4.16	3.2 ± 0.06	2
W-92	52.9096	-27.7277	2.98	24.49	26.57 ± 0.10	80 ± 5	5.2 ± 1.2	2.69	2.10 ± 0.04	5
W-101	52.9643	-27.7649	1.16	23.01	5.33 ± 0.10	34 ± 2.9	5.1 ± 1.3	0.66	2.53 ± 0.12	2
W-108	53.3175	-27.8445	1.75	17.36	516.74 ± 0.10	4040 ± 100 [c]	5.0 ± 1.2	7.89	0.0875	6
W-114	52.9628	-27.7436	3.11	23.88	51.63 ± 0.10	660 ± 9	4.9 ± 1.3	2.85	1.605	7

The columns are: (1) LABOCA source number in Weißet al. (2009); (2) X-ray counterpart Equatorial coordinates; (3) Total band X-ray flux in units of $\times 10^{-15}$ erg s^{-1}cm^{-2}; (4) R-band magnitude (AB) ; (5) 3.6μm flux in units of μJy; (6) 24μm flux in units of μJy ; notes: (a) Double source blended in the IRAC and/or MIPS PSFs; (b) nearby sources possibly affecting the measured flux (c) Lower limit (7) LABOCA 870 μm flux in units of mJy(8) Likelihood-ratio between LABOCA and MIPS counterpart (9) Redshift: Three and two decimal digits denote a spectroscopic and a photometric redshift respectively (10) Redshift reference: 1 EAZY; 2 Luo et al. (2010); 3 Szokoly et al. (2004); 4 Kriek et al. (2006); 5 Taylor et al. (2009); 6 Norris et al. (2006); 7 Chapin et al. (2010)

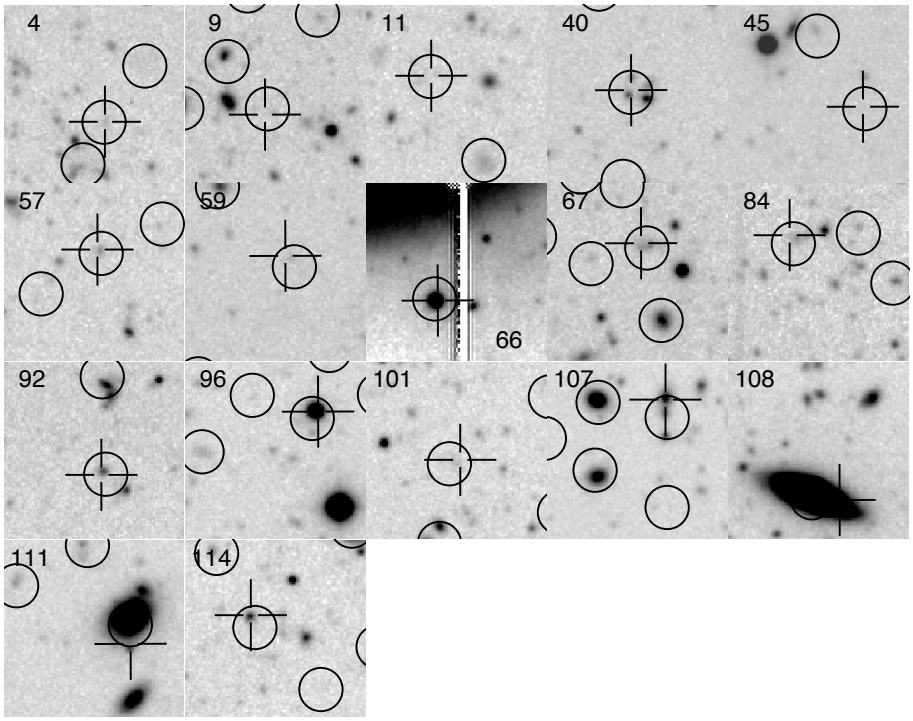

Fig. 1. The MUSYC R-band images. The circles (3 arcsec radius) show the MIPS positions while the crosses show the X-ray positions. The thumbnails are centered on the LABOCA coordinates while their size is 25 arcsec.

Apart from this first order approach, we fit a star-forming in combination with a torus template to the SED from 3.6 μm up to 870 μm. We use the SED templates of Polletta et al. (2007) in order to produce templates combining star formation and AGN activity. As star forming templates we use those of M 82 and Arp 220. These are two actively star forming galaxies differing in the star formation rate and the amount of dust. Arp 220 is producing stars with a rate of 270 $M_\odot$ yr^{-1} (Shioya et al. 2001) and its interstellar dust gives it an infrared luminosity $> 10^{12} L_\odot$, making it the prototypical ULIRG. M 82 on the other hand has a more modest star formation rate of 10 $M_\odot$ yr^{-1} and lower mid-to-far infrared luminosity. The two SEDs are almost identical in the near-to-mid infrared and differ significantly in their mid infrared PAH and silicate features and the mid-to-far infrared dust emission.

Table 2. X-ray spectral fits

ID	XID	z	N_H	Γ	N_H ($\Gamma = 1.8$)	Γ ($N_H = 0$)	L_X
(1)	(2)	(3)	(4)	(5)	(6)	(7)	(8)
W-4	LE-97	2.58	< 15.3	$1.55^{+2.14}_{-1.24}$	< 15.0	$1.56^{+1.67}_{-1.28}$	2.9
W–9	LU-114 LE-319	3.99	$28.3^{+8.5}_{-7.8}$	$1.72^{+0.16}_{-0.19}$	$31.1^{+4.2}_{-4.2}$	$1.04^{+0.10}_{-0.10}$	97.
W-11	LU-131 , LE-332	6.07	196^{+139}_{-93}	$2.32^{+0.47}_{-0.67}$	171^{+115}_{-74}	$1.02^{+0.38}_{-0.28}$	7.3
W-40	LU-385	1.90	-	-	$21^{+14.8}_{-13.6}$	$0.64^{+0.71}_{-0.79}$	1.1
W-45†	LU-230	2.50	-	-	< 5.53	$3.44^{+1.46}_{-1.23}$	0.37
W-57	LU-26, LE-203	2.940	$39.4^{+32.9}_{-26.5}$	$2.60^{+1.18}_{-1.01}$	$20.1^{+15.9}_{-12.9}$	$1.25^{+0.44}_{-0.54}$	6.8
W-59†	LU-441	1.38	-	-	< 6.1	$1.88^{+1.15}_{-0.88}$	0.12
W-66	LE-725	0.58	< 0.17	$2.04^{+0.25}_{-0.17}$	< 0.06	$2.07^{+0.18}_{-0.17}$	2.4
W-67†	LU-362	2.122	-	-	-	1.8	0.24
W-84	LU-33	3.20	< 30.5	$1.03^{+0.68}_{-0.49}$	$26.9^{+16.1}_{-7.6}$	$0.75^{+0.29}_{-0.27}$	7.3
W-92	LE-112	2.10	$3.6^{+21.0}_{-13.4}$	$0.33^{+1.53}_{-0.83}$	$34.7^{+25.1}_{-18.0}$	$0.10^{+0.66}_{-0.70}$	1.80
W-101	LU-25	2.53	< 7.9	$2.11^{+1.4}_{-0.6}$	< 2.8	$2.15^{+0.69}_{-0.62}$	1.53
W-108†	LE-634	0.0875	-	-	< 0.62	$4.3^{+2.63}_{-2.13}$	2×10^{-3}
W-114	LU-23	1.605	< 45.0	$-0.15^{+1.47}_{-1.02}$	$31.9^{+34.2}_{-12.6}$	$-0.42^{+0.54}_{-0.64}$	0.43

The columns are: (1) Laboca ID in Weißet al. (2009) (2) CDFS (LU) or eCDFS(LE) ID in Luo et al. (2008) or Lehmer et al. (2005) respectively (3) redshift; (4),(5) rest-frame column density and photon index in the case of sources with good photon statistics (see text) (6) rest-frame column density in units of 10^{22} cm^{-2} for fixed $\Gamma = 1.8$ (7) photon-index Γ for column density $N_H = 0$ (8) **Intrinsic** X-ray Luminosity in the 2-10 keV band in units of 10^{43} erg s^{-1} , obtained by setting $N_H = 0$ in column (6); † denotes a possible star-forming galaxies on the basis of the X-ray properties i.e. low X-ray luminosity and soft spectrum (see text).

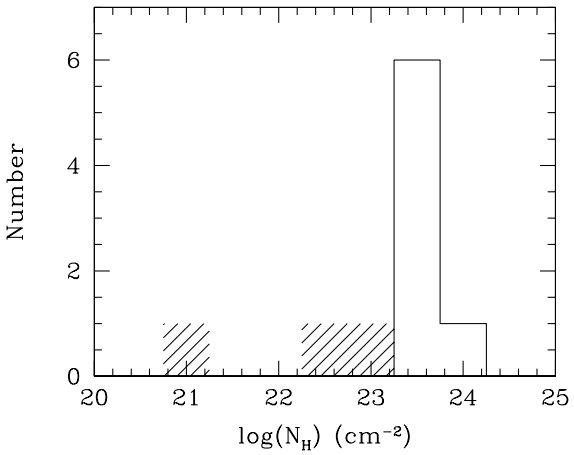

Fig. 3. The rest-frame column density distribution for the ten AGN (see text for details). The open and hatched histograms correspond to the detections and upper limits respectively.

As an AGN-only SED we use the Torus SED of Poletta et al. (2007), which is a fit to the SED of a heavily obscured type-2 QSO, SWIRE J104409.95+585224.8 (Polletta et al. 2006). We start the SED fitting by choosing the best linear combinations of Arp 220+Torus and M 82+Torus templates using the four IRAC and the 24 μm datapoints and minimizing the χ^2 value of the fit. Then we calculate the χ^2 values of the optimum combinations using the previous datapoints plus the sub-mm flux and choose the combination (Arp 220+Torus or M 82+Torus) which minimizes this value. In other words we use the mid-infrared to determine the relative AGN and starburst contribution (where the two starburst templates are almost identical) and define the optimum starburst template by its prediction of the far-infrared flux. Then, we use the F-test to determine whether the AGN contribution is needed to fit the mid-infrared flux; we calculate:

$$F = \frac{\frac{\chi_1^2 - \chi_2^2}{p_2 - p_1}}{\frac{\chi_2^2}{n - p_2}}$$

where χ_1^2 and χ_2^2 are the best-fit χ^2 values of the starburst-only and combination templates respectively, p_1 and p_2 are the degrees of freedom of the two cases (here $p_1 = 1$ and $p_2 = 2$) and n is the points used to make the fit (here $n = 5$). We assume that the AGN contribution is needed if the false-rejection probability is lower than 10% ($F > 8.5$).

The template fits are presented in Fig. 5, while the derived IR luminosities are given in Table 3. We note that the IR-luminosity is estimated from the mid-infrared SED and the 870 μm flux. This does not probe the peak of the infrared SED (around rest-frame 70μm in νF_ν) and thus introduces an appreciable uncertainty in the determination of the far-IR luminosity. Measurements of the infrared SED at its peak (for example with *Herschel*) are needed in order to provide accurate bolometric luminosities. However, we note that the 6 μm luminosities are hardly affected by the lack of far-IR measurements. We see that a torus component is required in most cases (eight out of ten AGN). However, the contribution of the torus to the total IR luminosity is small (see Table 3). The contribution of the torus is appreciable only in the case of the two power-law IRAC AGN (W-4 and W-57) and also in the case of the source W-11 (reaching up to $\sim 20\%$). For most candidate galaxies the bulk of the 6μm emission comes from star-forming processes. Only the can-

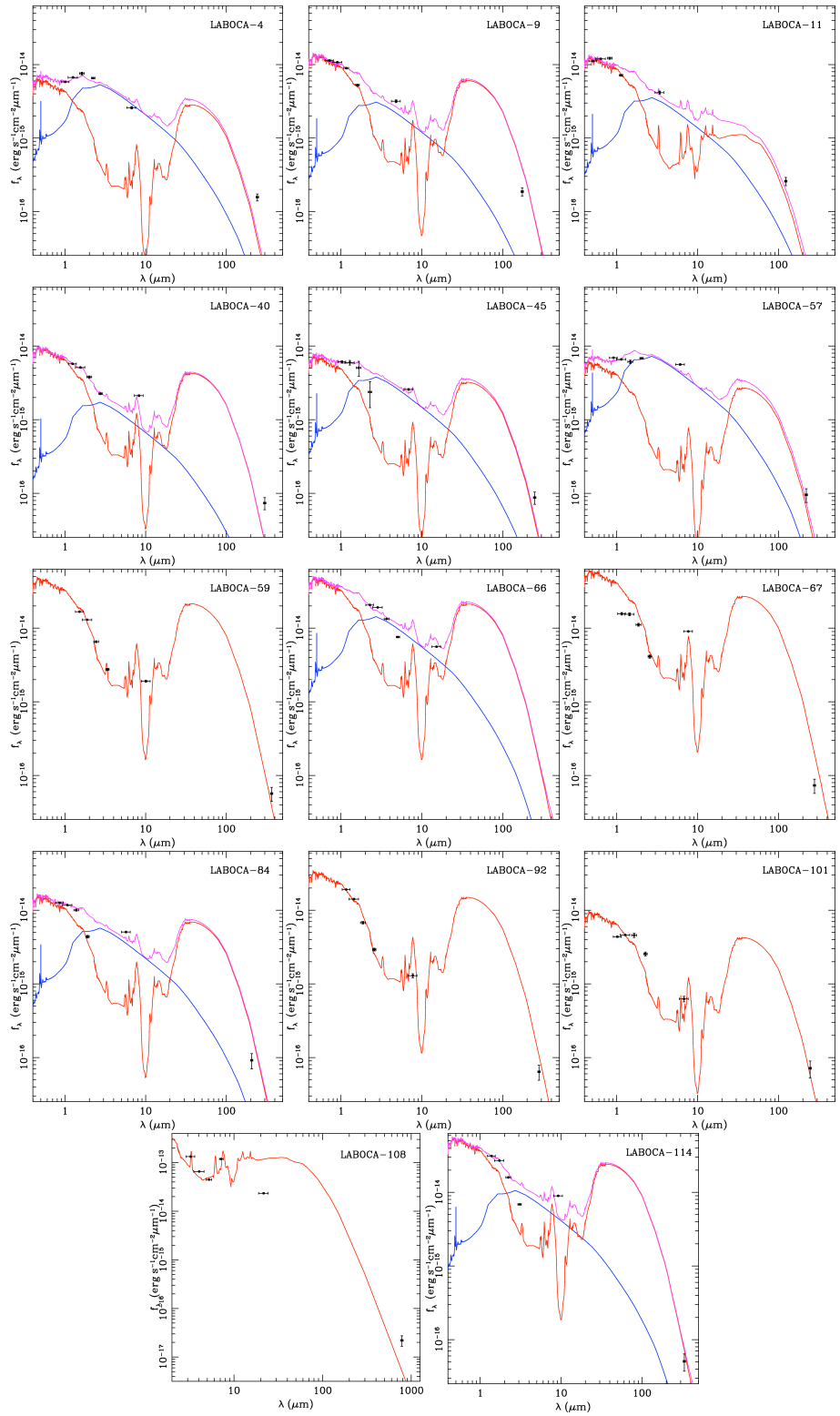

Fig. 5. IR through sub-mm Spectral Energy Distributions. The black points denote the observations while the solid lines the fitted templates: the red and blue lines represent the star-forming and torus templates of Polletta et al. (2007) while the purple curve denotes the total model

didate galaxy W-45 has a non-negligible torus component ($\sim 10\%$).

6.1.1. X-ray to 6 μm luminosity

The derivation of the $L_{\rm x}$ to $L_{6\,\mu{\rm m}}$ ratio has as a goal to identify any highly obscured, Compton-thick AGN. These are difficult to identify with X-ray spectroscopy especially

Table 3. Infrared Luminosities

ID	$\nu L_\nu(6\mu m)$	L_{IR}	L_{torus}/L_{IR}	$\log(L_X/L_{IR})$	IRAC	Full-SED	Prob.
(1)	(2)	(3)	(4)	(5)	(6)	(7)	(8)
W-4	1.0	1.4	0.14	-2.7	AGN	Arp220/Torus	0.5
W-9	1.7	7.8	0.04	-1.9	SF	Arp220/Torus	3.9
W-11	5.4	4.7	0.21	-2.8	SF	M82/Torus	2.1
W-40	0.16	0.88	0.03	-2.9	SF	Arp220/Torus	0.4
W-45†	0.69	1.4	0.09	-3.6	SF	Arp220/Torus	0.9
W-57	2.0	1.9	0.18	-2.4	AGN	Arp220/Torus	0.6
W-59†	0.06⋆	1.7	0.006	-4.15	SF	Arp220	42.
W-66	0.07	0.23	0.05	-1.98	SF	Arp220/Torus	3.9
W-67†	0.76⋆	4.2	0.03	-4.24	SF	Arp220	47.
W-84	1.9	5.3	0.07	-2.86	SF	Arp220/Torus	2.7
W-92	0.0⋆	3.8	0.00	-3.30	SF	Arp220	99.
W-101	0.22⋆	1.30	0.03	-2.92	SF	Arp220	11.1
W-108†	0.002⋆	0.02	0.03	-3.84	SF	M82	17.1
W-114	0.65⋆	3.3	0.03	-4.01	SF	Arp220/Torus	5.2

The columns are: (1) LABOCA ID as in Table 1 (2) Torus 6μm νL_ν monochromatic luminosity in units of 10^{45} erg s^{-1} . (3) 10-1000 μm Infrared Luminosity in units of 10^{46} erg s^{-1} . (4) Ratio of torus to total 10-1000 μm luminosity (5) Logarithm of the Ratio of X-ray luminosity to total IR (10-1000 μm) luminosity. (6) mid-IR IRAC template: power-law (AGN) vs. curved (star-forming) (7) Best-fit templates from Polletta et al. (2007). (8) Probability ($\times 10^{-2}$) that the torus component is not needed according to the F-test. Notes: (†) denotes a possible star-forming galaxy on the basis of the X-ray properties; ($\star$) means that the best-fit value of the torus luminosities are given although such component is not formally required by F-test.

in the case of limited photon statistics. One of the most reliable proxies of the intrinsic power of an AGN is the mid-IR monochromatic 6 μm luminosity (e.g. Lutz et al. 2004). This wavelength region is more representative of the hot dust heated by the AGN and thus provides a reliable diagnostic of the AGN power (e.g. Alexander et al. 2008).

We present the 2-10 keV absorbed luminosity against the monochromatic 6 μm IR luminosity coming from the torus in Fig. 6. The area between the solid lines denotes the region of the X-ray to 6 μm luminosity plane where local AGN reside (Lutz et al. 2004, Alexander et al. 2008, Bauer et al. 2010). The area below the dashed line corresponds to low X-ray luminosity sources, i.e. Compton-thick sources (or alternatively normal galaxies). We see that some sources fall in the low part of the $L_x/L_{6\,\mu m}$ diagram (e.g. W-11, W-57, W-114). All four candidate galaxies, i.e. the sources with low X-ray luminosities and soft X-ray spectra fall as well in the low part of this diagram.

7. X-ray Stacking Analysis

Having dealt with the properties of the X-ray detected SMGs, we attempt to gain an insight on the average X-ray properties of the individually undetected LABOCA sources. This can be done in a statistical manner simply by co-adding (stacking) the X-ray flux around each SMG. Stacking techniques have been widely used in X-ray Astronomy to study the mean properties of source populations selected to have certain well defined properties and which are too faint in X-rays to be individually detected (e.g. Nandra et al. 2002; Georgantopoulos et al. 2008). A fixed radius aperture is used to extract and to sum the X-ray photons at the positions of the LABOCA sources. Sources that lie close to or are associated with an X-ray detection are excluded from the analysis to avoid contamination of the stacked signal from the X-ray photons of detected sources. In order to maximise the signal we adopt an extraction radius of 3 arcsec around the MIPS 24 μm counterparts of the LABOCA sources. A 3 arcsec aperture encloses more than about 90% of the photons in the soft 0.5-2 keV spectral band at an off-axis angle of 5 arcmin. We perform the stacking analysis in two energy bands: the soft (0.5-2 keV) and the hard (2-5 keV). The choice of the latter band minimises the instrumental background contamination thus maximising the sensitivity of the stacking analysis. We perform the stacking analysis for the LABOCA sources lying in both the eCDFS and CDFS regions.

The significance of the stacked signal depends on the value of the background. This is estimated by using the background maps produced by the WAVDETECT task of CIAO. We sum the X-ray photons in regions around each source used in the stacking. The significance of the stacked signal in background standard deviations is estimated by (T - B) / T, where T and B are the total (source + background) and background counts respectively. Fluxes are determined by multiplying the stacked count rate by the appropriate energy conversion factor, which is estimated separately for each class of sources, based on the spectral shape of the stacked signal. A rough estimate of the mean spectral index is obtained by deriving the hardness ratio (HR=(h-s)/(h+s)) between the s=0.5-2 keV and h=2-5 keV bands.

The stacking results are summarised in Table 4. We see that the stacking of the LABOCA sources in the eCDFS reveals a strong signal in the soft band while the signal is marginal in the hard band. We have checked the significance of the soft signal by performing 100 simulations around random positions on the image. There is no simulation where we obtain a signal higher than the actually detected signal (61 counts), implying that the confidence limit for our detection is higher than 99%. The implied flux in the soft band is 2.3×10^{-17} erg cm^{-2} s^{-1}, i.e. about four times fainter than the flux limit in the eCDFS (see Virani et al. 2008, Lehmer et al. 2005). We find a hardness ratio of -0.40 ± 0.10 corresponding to a photon index of $\Gamma \approx 1.6$. We note that in the CDFS we barely detect a signal even in

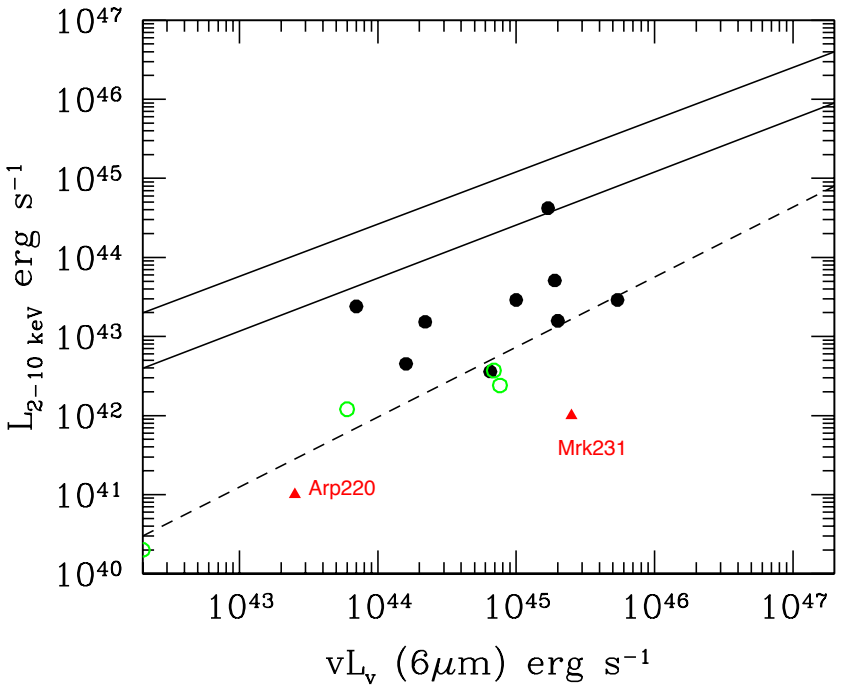

Fig. 6. The X-ray (2-10 keV) luminosity (uncorrected for absorption) as a function of the torus 6μm luminosity. Filled (black) circles represent the AGN while open (green) circles denote the candidate galaxies. Note that only nine AGN are plotted as source W-92 shows no torus contribution. The solid lines denote the region occupied by unabsorbed AGN while the region beyond the short dash line is populated by Compton-thick AGN in the local Universe (adapted from Alexander et al. 2008). For comparison we plot the positions of Arp220 and the Compton-thick AGN Mrk231 on the diagram.

Table 4. X-ray Stacking Results

Sample	No	Soft Counts	Soft Flux	Hard Counts	Hard Flux	HR
(1)	(2)	(3)	(4)	(5)	(6)	(7)
LABOCA eCDFS	100	61 (5.6σ)	2.3×10^{-17}	26 (2.2σ)	2.2×10^{-17}	-0.40 ± 0.10
LABOCA CDFS	21	28 (2.5σ)	5×10^{-18}	16 (1.3σ)	$< 1.6 \times 10^{-17}$	$> -0.06^{\dagger}$

(1), (2) sample where stacking technique has been applied and number of sources. (3) Net soft counts and significance of signal. (4) Soft flux (0.5-2 keV) in units of erg cm^{-2} s^{-1} . (5) Hard net counts and significance. (6) Hard flux (2-5 keV) in units of erg cm^{-2} s^{-1} . (7) Hardness ratio. (†): the upper limit on flux and the corresponding lower limit on the hardness ratio correspond to 2σ.

the soft band. This is most probably because of the small number of SMGs employed in the stacking analysis.

8. Discussion

In the previous sections we presented a comprehensive analysis of the X-ray and mid-IR properties of the SMG galaxies in the eCDFS and CDFS. These properties are used to assess (1) the fraction of AGN among the SMG population (2) the amount of obscuration and in particular Compton-thick obscuration (3) The power-mechanism among the SMG which host an AGN

8.1. Fraction of AGN among SMGs

Using robust positions from *Spitzer* MIPS, we find 14 associations of X-ray sources with LABOCA SMGs or a fraction of (11 ± 3 %). As the observations in the area of the CDFS are very sensitive, it is very likely that a significant number of sources are associated with normal galaxies rather than AGN (see Hornschemeier et al. 2003, Tzanavaris &

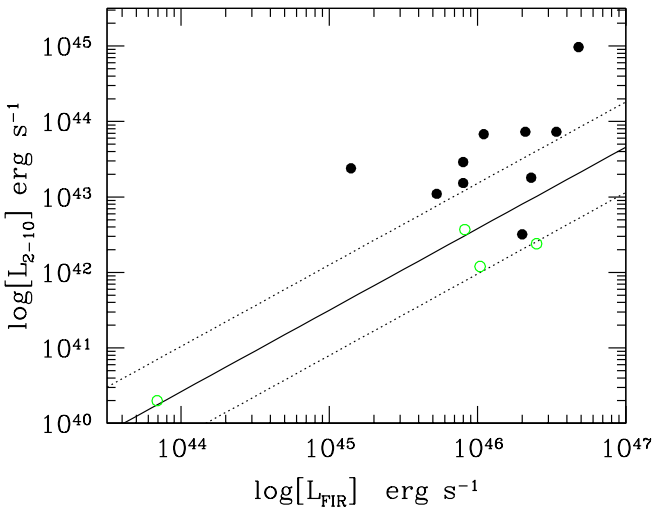

Fig. 7. The X-ray (2-10 keV) vs. the FIR (4-100 μm) relation for our sources. The solid and dotted lines denote the best-fit relation of Ranalli et al. (2003) - and its associated 2σ error, for normal galaxies in the local Universe. Open circles denote the four sources classified as galaxies on the basis of the X-ray diagnostics.

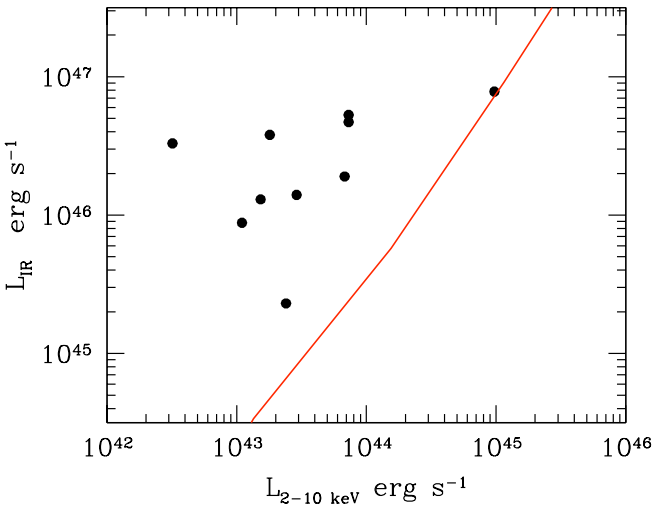

Fig. 8. The X-ray (2-10 keV) vs. the total IR (10-1000 μm) luminosity relation for our sources. The solid line denotes the empirical relation of Hopkins et al. (2007) for the bolometric correction of AGN.

Georgantopoulos 2008, Ptak et al. 2008 and references therein). The X-ray analysis has suggested that a number (four) of SMGs are associated with normal galaxies rather than AGN. This was based on their relatively low X-ray luminosities (less than a few times 10^{42} erg s^{-1}) in combination with unobscured X-ray spectra. A further check on whether these sources are associated with normal galaxies can be provided by the $L_{\rm x} - L_{\rm FIR}$ relation of Ranalli et al. (2003). These authors have found a strong correlation between the X-ray and the IR luminosity in star-forming galaxies in the local Universe. This implies that only sources with an excess of X-ray emission above this relation can

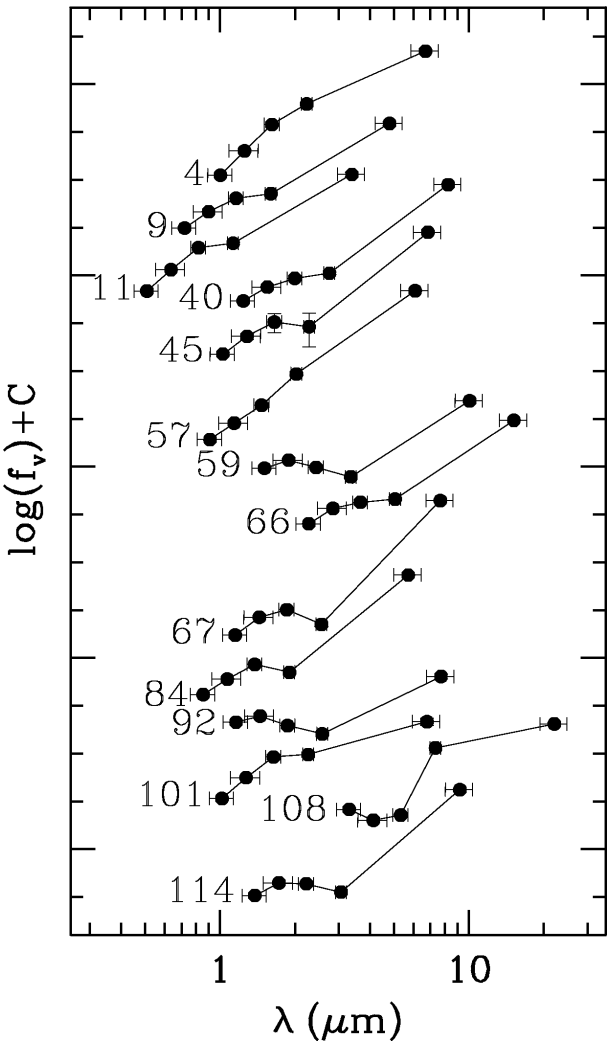

Fig. 4. The IRAC, MIPS (24μm) Spectral Energy Distributions

be securely associated with AGN. We show this relation in Fig. 7. It can be seen that the four sources classified as galaxies on the basis of the X-ray diagnostics alone also follow the $L_{\rm x} - L_{\rm FIR}$ relation of Ranalli et al. (2003). A fifth source which falls below the Ranalli et al. (2003) relation has a flat spectrum and thus is most probably an AGN (W-114).

Excluding the four candidate galaxies, the fraction of X-ray detected AGN among the LABOCA SMGs amounts to 10/126 (8 ± 2)%. Constraining this analysis in the CDFs where the sensitivity is the highest yields a higher AGN fraction, as expected. In particular, there are 38 LABOCA sources in CDFS; out of these, ten are associated with X-ray sources translating to a percentage of X-ray detections of (26 ± 9)%. As among these ten sources, three are most likely associated with galaxies, a conservative estimate for the AGN fraction amounts to 7/38 (18 ± 7)%.

We compare the figures above with the fraction of X-ray sources and AGN in particular that Alexander et al. (2005b) and Laird et al. (2010) have derived in the CDFN. As the X-ray sensitivity of the CDFS and CDFN are identical this comparison is straightforward. Alexander et al. (2005b) find a very high fraction of X-ray detections among radio-detected SMGs $(75 \pm 19\%)$. Laird et al. (2010) find a lower fraction of X-ray detections among the overall SMG population $(45 \pm 8$ %). The primary difference between the analysis of Laird et al. (2010) and that of Alexander et al. (2005b) is that the former uses a purely sub-mm selected sample (Pope et al. 2006) while the latter employs a mixture of SMGs and radio sources with follow-up SCUBA photometry. Therefore the sample of Laird et al. (2010) which contains 35 SMGs is more appropriate for comparison with our work. Although this sample gives a higher fraction of X-ray detections compared with our sample, their AGN fraction of about 25±8 % is in reasonable agreement with the results presented here.

The AGN fraction derived here can be considered only as a lower limit to the true AGN fraction. This is because there may be many more low luminosity (for example obscured) AGN among the non-X-ray detected SMGs. The X-ray stacking analysis could shed more light on such a possibility. A strong signal is detected in the soft band in the eCDFS with a corresponding flux of 2×10^{-17} erg cm^{-2} s^{-1} . If we adopt the average redshift of the non X-ray detections in the SMG sample of Pope et al. (2006) (z=2.1) as the median redshift of our non X-ray detected SMGs, we find that their X-ray luminosity amounts to 5×10^{41} erg s^{-1} . The luminosity obtained above is comparable to that obtained by Laird et al. (2010) for their X-ray undetected SMGs in the soft band (4×10^{41} erg s^{-1}). The hardness ratio of -0.40±0.10 shows relatively little absorption. In particular, this hardness ratio corresponds to $N_{\rm H} = 1 \times 10^{21}$ cm^{-2} at the observer's frame assuming a photon index of $\Gamma = 1.8$ (or $N_{\rm H} \approx 2 \times 10^{22}$cm^{-2} at z=2). Alternatively, this hardness ratio corresponds to a photon-index of $\Gamma \approx 1.6$ (for $N_{\rm H} = 0$). Given that the implied spectrum is relatively unobscured, it is reasonable to assume that the bulk of the X-ray emission comes from star-forming processes and to estimate the star-formation-rate (SFR). As the IR luminosity provides a robust measurement of the star-formation rate (SFR), the tight $L_{\rm x} - L_{\rm FIR}$ correlation found by Ranalli et al. (2003) implies that X-rays are also a good tracer of the star-formation in galaxies. Based on their $L_X - L_{IR} - SFR$ correlation, we find an average SFR of 110 M$_\odot$ yr^{-1} for our non-X-ray detected sources. This is in agreement with the value derived by Laird et al. (2010) namely 150M$_\odot$yr^{-1}. As these authors point out, this value is well below the huge SFR ($\sim$ 1000M$_\odot$yr^{-1} which have been derived for SMGs on the basis of the FIR luminosities. This is also below the SFR derived for the three most luminous candidate galaxies in our sample (W-45, W-59 and W-67) which ranges between $\sim$ 300-1000 M$_\odot$yr^{-1}, according to the X-ray luminosity and the relation of Ranalli et al. (2003). It is rather unlikely that the low SFR derived from the stacked signal in SMGs can be attributed to obscured star-formation. For example, if the column density is $N_{\rm H} \sim 10^{22}$cm^{-2} at z=2 as suggested above, the 0.5-2 keV luminosity and thus the SFR would increase by a factor of only 1.5.

8.2. Obscuration

The direct X-ray spectral analysis reveals that the majority of AGN are significantly absorbed having column densities above 10^{23} cm^{-2} (see Fig. 3). One of the sources could be even classified as a transmission dominated Compton-thick AGN: this is W-11 at a photometric resdhift of z=6.07. Nevertheless, this classification is highly ambiguous because

of the associated redshift uncertainties. The $L_{\rm x} - L_{6\,\mu{\rm m}}$ diagram suggests that source W-114 may be related to a reflection-dominated Compton-thick source. Its flat X-ray spectrum ($\Gamma < 1.32$ at the 90% confidence limit) is also pointing towards this interpretation. Our results on the amount of obscuration are in reasonable agreement with those of Laird et al. (2010) in the CDFN. These authors find seven bona-fide AGN among their 18 SMG/X-ray associations. Their X-ray spectral analysis shows a median obscuration of $\sim 10^{23}\,{\rm cm}^{-2}$ with one of their sources being a Compton-thick AGN.

The stacking analysis provides significant constraints on the fraction of Compton-thick sources among the SMG undetected in X-rays. The detected signal is relatively soft (hr=-0.40 between the 0.5-2 keV and the 2-5 keV bands), implying a spectrum with a photon index of $\Gamma = 1.6$. This immediately suggests a small fraction of hard spectrum sources such as those associated with Compton-thick AGN. In order to quantify the fraction of Compton-thick AGN, we assume a simplistic model where the undetected SMG population consists solely of star-forming galaxies and Compton-thick AGN. We assume that normal galaxies have an average spectrum of $\Gamma = 1.7$, (e.g. Zezas et al. 1998) which corresponds to a hardness ratio of -0.44 in the above spectral bands. We further adopt that Compton-thick sources have a spectrum of $\Gamma = 1$ (e.g. Matt et al. 2004, Georgantopoulos et al. 2009) or equivalently a hardness ratio of -0.13. We derive a fraction of Compton-thick sources of about 10%. We point out that this estimate is valid only under the assumption that the X-ray fluxes from all the sources are roughly the same. This fraction should only be considered as an upper limit. In the case where there exist AGN with significant obscuration (but not necessarily Compton-thick) among the undetected SMG sources, the fraction of Compton-thick sources will be lower. For example, AGN with a rest-frame column density of $N_{\rm H} = 10^{23}\,{\rm cm}^{-2}$ at z=2 have a hardness ratio similar to that of a reflection-dominated Compton-thick AGN with $\Gamma = 1$.

8.3. The SMG power-mechanism

We discuss here the possibility that the AGN powers the total IR emission in the case of our ten bona-fide AGN, i.e. we exclude the four sources classified as possible galaxies on the basis of low X-ray luminosities and soft X-ray spectra (see section 8.1 above). The SED fitting provides a clear picture of the AGN contribution. We find that even in the two sources which have power-law IRAC photometric distributions and thus are clearcut AGN in the mid-IR part of the spectrum, the torus contributes less than 20% of the total IR (10-1000 μm) luminosity. Laird et al. (2010) estimate a fraction of 3/16 for AGN-powered SMGs in their sample.

In order to better visualize the level of the AGN contribution, we plot the total IR luminosity as a function of the X-ray luminosity in Fig. 8 for our sources together with the empirically estimated relation for AGN (Hopkins et al. 2007). We see that only one source (W-9) follows this relation, while the remaining sources are far above the relation of Hopkins et al. (2007), implying a negligible AGN contribution.

9. Conclusions

We explore the X-ray properties of the 126 sub-mm sources of the LABOCA survey in the area of the CDFS and eCDFS. Using *Spitzer* and radio counterparts of the sub-mm sources where available, we find 14 sources with significant X-ray detection. Our results can be summarised as follows:

- The X-ray luminosities and spectra suggest that most of the sub-mm - X-rays associations (10/14) host an AGN. In four sources the X-ray emission could possibly originate from star-forming processes.
- The fraction of X-ray AGN among the LABOCA SMG sample in the area of the CDF-S is at most 26 ± 9 %.
- Six of our X-ray sources show significant amounts of absorption $N_{\rm H} > 10^{23}$ cm^{-2} but there is no unambiguous evidence that any of the sources is a Compton-thick AGN.
- Detailed SED fitting shows that most of the AGN require a torus component. However, the AGN contribution to the total IR luminosity is small.
- X-ray stacking analysis of the undetected SMGs reveals a signal with a relatively soft spectrum. This is more suggestive of a SFR galaxy population.

Acknowledgements. IG and AC acknowledge the Marie Curie fellowship FP7-PEOPLE-IEF-2008 Prop. 235285. AC acknowledges receipt of ASI grants I/023/05/00 and I/88/06. We acknowledge the use of *Spitzer* data provided by the *Spitzer* Science Center. The Chandra data were taken from the Chandra Data Archive at the Chandra X-ray Center.

References

Alonso-Herrero, A., Pérez-González, P. G., Alexander, D. M., et al. 2006, ApJ, 640, 127
Armus, L., Charmandaris, V., Bernard-Salas, J. et al. 2007, ApJ, 656, 148
Arnaud, K.A., 1996, Astronomical Data Analysis Software and Systems V, eds. Jacoby, G. & Barnes, J., ASP Conf. Series, 101, 17
Alexander, D. M., Bauer, F. E., Brandt, W. N., et al., 2003, AJ, 126, 539
Alexander, D.M., Smail, I., Bauer, F.E., Chapman, S. C., 2005, Nature, 434, 738
Alexander, D.M., Bauer, F.E., Chapman, S.C. et al., 2005, ApJ, 632, 736
Alexander, D.M., Chary, R.R., Pope, A. et al. 2008, ApJ, 687, 835
Aretxaga, I., Hughes, D.H., Coppin, K., et al., 2007, MNRAS, 376, 1571
Barger, A.J., Cowie, L.L., Sanders, D.B., Fulton, E., Taniguchi, Y., Sato, Y., Kawara, K., Okuda, H., 1998, Nature, 394, 248
Bauer, F.E., Yan , L., Sajina, A., Alexander, D.M., 2010, ApJ, 710, 212
Bertin, E., Arnouts, S., 1996, A&AS, 117, 393
Blain, A.W., Smail, I., Ivison, R.J., Kneib, J.-P., 1999, MNRAS, 302, 632
Blain, Andrew W., Smail, I., Ivison, R.J., Kneib, J.-P., Frayer, David T., 2002, PhR, 369, 111
Braito, V., Della Ceca, R., Piconcelli, E., et al., 2004, A&A, 420, 79
Brammer, G. P., van Dokkum, P. G., Coppin, P., 2008, ApJ, 686, 1503
Capak, P., Carilli, C. L., Lee, N., Aldcroft, T., et al. 2008, ApL, 681, L53
Cash, W., 1979, ApJ, 228, 939
Chapin, E.L., Chapman, S.C., Coppin, E., et al., 2010, astro-ph/1003.2647
Chapman, S.C., Blain, A. W., Smail, I., Ivison, R. J., 2003
Chapman, S.C., Blain, A. W., Smail, I., Ivison, R. J., 2005, ApJ, 622, 772
Coppin, K.E.K., Smail, I., Alexander, D. M., et al. 2009, MNRAS, 395, 1905

Daddi, E., Dannerbauer, H., Stern, D., Dickinson, M., et al., 2009, ApJ, 694, 1517
Dickey, J. M., Lockman, F. J., 1990, ARA&A, 28, 215
Dickinson, M., Giavalisco, M., The Goods Team., 2003, in The Mass of Galaxies at Low and High Redshift, ed. R. Bender & A. Renzini, Springer-Verlag, 324
Dickinson, M., Alexander, D., Bell, E., et al., 2006, sptz.prop, 30948
Donley, J. L., Rieke, G. H., Pérez-González, P. G., Barro, G., 2008, ApJ, 687, 111
Gawiser, E., van Dokkum, P. G., Herrera, D., et al., 2006, ApJS, 162, 1
Georgakakis, A., Georgantopoulos, I., Akylas, A., Zezas, A., Tzanavaris, P., 2006, ApJ, 641, L101
Georgakakis, A., Rowan-Robinson, M., Babbedge, T.S.R., Georgantopoulos, I., 2007, MNRAS, 377, 203
Georgantopoulos, I., Georgakakis, A., Rowan-Robinson, M., Rovilos, E., 2008, A&A, 484, 671
Georgantopoulos, I., Akylas, A., Georgakakis, A., Rowan-Robinson, M., 2009, A&A, 507, 747
Giacconi, R., Zirm, A., Wang, J., et al., 2002, ApJS, 139, 369
Giavalisco, M., Ferguson, H. C., Koekemoer, A. M., et al., 2004, ApJ, 600, 93
Grazian, A., Fontana, A., de Santis, C., et al., 2006, A&A, 449, 951
Güsten, R., Nyman, L.A., Schilke, P., Menten, K., Cesarsky, C., Booth, R., 2006, A&A, 454, L13
Hopkins, P.F., Richards, G.T., Hernquist, L., 2007, ApJ, 654, 731
Hornschemeier, A.E., Bauer, F.E., Alexander, D.M., et al. 2003, AJ, 126, 575
Hughes, D.H., Serjeant, S., Dunlop, J., et al. 1998, Nature, 394, 241
Iwasawa, K., Sanders, D.B., Evans, A.S., Trentham, N., Miniutti, G., Spoon, H.W.W., 2005, MNRAS, 357, 565
Kellermann, K. I., Fomalont, E. B., Mainieri, V., Padovani, P., Rosati, P., Shaver, P., Tozzi, P., Miller, N., 2008, ApJS, 179, 71
Kriek, M., van Dokkum, P. G., Franx, M., et al., 2006, ApJ, 649, L71
Laird, E.S., Nandra, K., Pope, A., Scott, D., 2010, MNRAS, 401, 2763
Lehmer, B.D., Brandt, W.N., Alexander, D.M., et al., 2005, ApJS, 161, 21
Luo, B., Bauer, F.E., Brandt, W.N., et al. 2008, ApJS, 179, 19
Luo, B., Brandt, W.N., Xue, Y.Q., et al. 2010, arxiv/1002.3154
Lutz, D., Maiolino, R., Spoon, H. W. W., Moorwood, A. F. M., 2004, A&A, 418, 465
Lutz, D., Mainieri, V., Rafferty, D., et al., 2010, ApJ, 712, 1287
Magnelli, B., Elbaz, D., Chary, R.R., et al., 2009, A& A, 496, 57
Maiolino, R., 2008, NewA, 52, 339
Matt, G., Bianchi, S., Guainazzi, M., Molendi, S., 2004, A& A, 421, 473
Menéndez-Delmestre, K., Blain, A.W., Alexander, D.M., et al. 2007, ApJ, 655, L65
Menéndez-Delmestre, K., Blain, A.W., Smail, I., et al. 2009, ApJ, 699, 667
Moran, E.C., Lehnert, Matthew D., Helfand, D.J., 1998, ApJ, 526, 649
Nandra, K., & Pounds, K., 1994, MNRAS, 268, 405
Nandra, K., Mushotzky, R.F., Arnaud, K., Steidel, C.C., Adelberger, K. L., Gardner, J.P., Teplitz, H.I., Windhorst, R. A., 2002, ApJ, 576, 625
Polletta, M., Wilkes, B. J., Siana, B., et al., 2006, ApJ, 642, 673
Polletta, M., Tajer, M., Maraschi, L., et al., 2007, ApJ, 663, 81
Pope, A., Scott, D., Dickinson, M., et al. 2006, MNRAS, 370, 1185
Pope, A., Chary, R.-R., Alexander, D.M., 2008, ApJ, 675, 1171
Ptak, A., Mobasher, B., Hornschemeier, A., Bauer, F., Norman, C., 2007, ApJ, 667, 826
Ranalli, P., Comastri, A., Setti, G., 2003, A&A, 399, 39
Rovilos, E., Georgantopoulos, I., Tzanavaris, P., Pracy, M., Whiting, M., Woods, D., Goudis, C., 2009, A&A, 502, 85
Rovilos, E., Georgantopoulos, I., Akylas, A., Fotopoulou, S., 2010, arxiv/1006.0746
Rix, H.-W. Barden, M., Beckwith, S.V.W. et al. 2004, ApJS, 152, 163
Shao, L., Lutz, D., Nordon, R. et al., 2010, astro-ph/1005.2562
Shioya, Y., Taniguchi, Y., Trentham, N., 2001, MNRAS, 321, 11
Siringo, G., Kreysa, E., Kovács, A., et al. 2009, A&A, 497, 945
Smail, I., Ivison, R.J., Blain, A.W., 1997, ApJ, 490, L5
Sutherland, W., Saunders, W., 1992, MNRAS, 259, 413
Szokoly, G. P., Bergeron, J., Hasinger, G., et al., 2004, ApJS, 155, 271
Taylor, E. N., Franx, M., van Dokkum, P. G., et al., 2009, ApJS, 183, 295
Tozzi, P., Gilli, R., Mainieri, V. et al. 2006, A&A, 451, 457
Tzanavaris, P., Georgantopoulos, I., Georgakakis, A., 2006, A&A, 454, 447
Tzanavaris, P. & Georgantopoulos, I., 2008, A& A, 480, 663
Valiante, E., Lutz, D., Sturm, E., Genzel, R., Tacconi, L.J., Lehnert, M.D., Baker, A.J., 2007, ApJ, 660, 1060
Virani, S.N., Treister, E., Urry, C. M., Gawiser, E., 2006, AJ, 131, 2373
Wall, J.V., Pope, A., Scott, D., 2008, MNRAS, 383, 435
Wardlow, J.L., Smail, I., Coppin, K.E.K. et al. 2010, astro-ph/1006.2137
Weiß, A., Kovács, A., Coppin, K., et al., 2009, ApJ, 707, 1201
Werner, M.W., 2000, SPIE, 4131, 1
Zezas, A.L., Georgantopoulos, I., Ward, M.J., 1998, MNRAS, 301, 915